Formation of Ge nanocrystals embedded in a SiO_2 matrix: Transmission electron microscopy, x-ray absorption, and optical studies

A. V. Kolobov,[1,*] S. Q. Wei,[2] W. S. Yan,[2] H. Oyanagi,[3] Y. Maeda,[4] and K. Tanaka[5]

[1]*Laboratory for Advanced Optical Technology (LAOTECH), National Institute of Advanced Industrial Science and Technology (AIST), Tsukuba Central 4, 1-1-1 Higashi, Ibaraki 305-8562, Japan*

[2]*National Synchrotron Radiation Laboratory, University of Science and Technology of China, Hefei, Anhui 230026, People's Republic of China*

[3]*Photonic Institute, National Institute of Advanced Industrial Science and Technology, Tsukuba Central 2, 1-1-1 Umezono, Ibaraki 305-8568, Japan*

[4]*Osaka Prefecture University, 1-1 Gakuencho, Sakai, Osaka 599-8531, Japan*

[5]*National Institute of Advanced Industrial Science and Technology, Tsukuba Central 4, 1-1-1 Higashi, Tsukuba, Ibaraki 305-8562, Japan*

(Received 29 July 2002; revised manuscript received 6 March 2003; published 13 May 2003)

The structure of Ge nanocrystals embedded into a SiO_2 matrix on either Si(100) or quartz-glass substrates has been studied by transmission electron microscopy, x-ray absorption fine structure, and Raman scattering. The size of the nanocrystals (5–20 nm) is found to strongly depend on the substrate material, while their shape—either spherical nanocrystals with multiple twinning defects or faceted single crystals—depends on the location of the nanocrystals in the matrix. We found that Ge nanocrystals are predominantly formed from the amorphous Ge phase, preexisting in the samples with higher Ge concentration, the formed nanocrystals are randomly oriented and have a Ge–Ge bond length of 2.45 ± 0.01 Å, i.e., are relaxed.

DOI: 10.1103/PhysRevB.67.195314 PACS number(s): 78.67.Bf, 68.37.Lp, 61.10.Ht, 78.30.Fs

I. INTRODUCTION

Si and Ge nanocrystals (nc-Si,Ge) embedded in SiO_2 have recently attracted much attention due to their possible applications in integrated optoelectronic devices.[1–4] In particular, it has been suggested that in small-size group-IV nanocrystals direct optical transitions are possible.[5] It was argued, based on comparison of Si and Ge effective masses and energy differences between the indirect gap and direct gap, that it should be easier to modify the electronic structure around the band gap of Ge.[6]

One of the promising ways to fabricate Ge nanostructures is to make embedded Ge nanocrystals, the matrix usually being SiO_2. Different techniques, such as co-sputtering and ion implantions,[7–9] and subsequent annealing are the usual way to produce the nanocrystals. Intense visible photoluminescence (PL) from Ge nanostructures has indeed been reported.[10,11]

The structure of nanocrystals is usually investigated using Raman scattering spectroscopy. While this is a powerful technique, in the particular case of Ge nanostructures grown on Si substrates it has to be applied with much care. We have demonstrated earlier[12,13] that in many cases the experimentally observed peak at ~ 300 cm^{-1} arises in fact from the Si substrate.

A technique ideally suitable to determine the local structure is x-ray absorption spectroscopy. Analysis of extended x-ray absorption fine structure (EXAFS) allows one to determine the bond length (with an accuracy of up to 0.005 Å), coordination number, and degree of disorder [mean-square relative displacement (MSRD)]. X-ray absorption near-edge structure (XANES) spectra, in addition to the local atomic structure, provide information on the electronic states.[14] Advantages of XANES over the often used x-ray photoemission spectroscopy (XPS) to characterize the degree of oxidation are (1) bulk rather than surface sensitivity and (2) a smaller degree of the sample charging during the measurement.

In this paper we first present transmission electron microscopy (TEM) images of the formed nanocrystals that provide direct evidence of the nanocrystal formation. We further describe in detail the results of x-ray absorption studies of embedded Ge nanocrystals. We finally compare the conclusions based upon these results with those obtained from optical measurements.

II. EXPERIMENTAL DETAILS

Our samples were prepared by co-deposition of Ge and SiO_2 by radio-frequency (rf) magnetron sputtering onto either quartz glass or Si(100) substrates with about 3–5-nm-thick native oxide. The thickness of the samples was in a 500-nm to 1-μm range and the Ge concentration varied from 25 to 60 mol %. After deposition, the samples were annealed for 1 h at 800 °C in an argon atmosphere which produced nanocrystals. More details on the sample preparation can be found elsewhere.[6] Below we shall refer to different samples as Ge$\langle\cdots\rangle$/substrate, with the number within the angular brackets denoting the Ge concentration. Thus the notation Ge$\langle 25\rangle$/Si(100) corresponds to the sample with 25 mol % Ge in the SiO_2 matrix on a Si(100) substrate. TEM images were taken on a Hitachi H-9000 instrument with an accelerating voltage of 300 kV.

X-ray absorption measurements were performed in the fluorescence mode at room temperature at beam line BL13B of the Photon Factory. As the fluorescence x-ray detector, we have used a 19-element pure Ge detector. Typical count rates were about 20 000 count/sec. A double-crystal Si(111) monochromator designed for a high-heat-load wiggler was used. Higher-order harmonics were minimized by detuning the

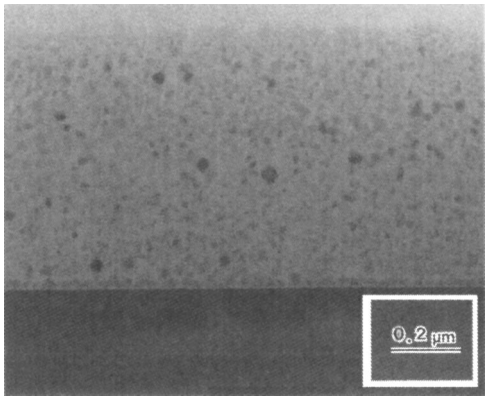

FIG. 1. TEM image of the annealed Ge⟨60⟩/Si(100) sample.

Si(111) crystal monochromator to about 70% of maximum incident intensity. The measured energy resolution at the Cu *K*-edge (8.980 keV) was 2.0 eV with a partially limited vertical beam size. Extrapolating the function, the energy resolution is expected to be about 4 eV at the Ge *K*-edge energy.

The stability of energy position was monitored by the independent XANES measurements of reference materials, i.e., copper foil and bulk *c*-Ge, the former being the calibration point. It was found that the energy scale was stable during the experiment, extending up to 6 days within $\pm 0.0002°$ in Bragg angle, which amounts to about 0.57 eV in uncertainty. For XANES spectra, measurements were sequentially performed during the same fill for which uncertainty in the energy scale was estimated to be less than 0.5 eV. More details on the experimental equipment can be found elsewhere.[15]

As references, we have used a thick (about 1 μm) film of Ge grown by molecular beam epitaxy on Si(100) (measured in fluorescence mode) and tetragonal GeO_2 (measured in transmission mode). Raman scattering was done at room temperature using 633 and 514 excitation wave lengths.

III. EXPERIMENTAL RESULTS

A. Transmission electron microscopy

Figure 1 shows the TEM image of the annealed Ge⟨60⟩/Si(100). One can clearly see the formed nanocrystals. Interestingly, the nanocrystals are preferentially formed in the area away from the sample surface. One can also see that at the interface with the silicon substrate the density of the nanocrystals is somewhat higher.

High-resolution (HR) TEM images (Fig. 2, top and middle) reveal several other features of the formed nanocrystals. The nanocrystals formed in the bulk of the sample have clearly pronounced facets and are single crystals, in a few cases with twinning defects. The nanocrystals formed in the direct vicinity of the Si substrate, on the other hand, are spherical and the interface under these nanocrystals is no longer flat. The size of the nanocrystals is almost the same in both cases and is about 20 nm.

In the sample with lower Ge content, the nanocrystal size is found to be smaller, in particular, in the annealed Ge⟨40⟩/Si(100) sample, their size is ~8 nm.

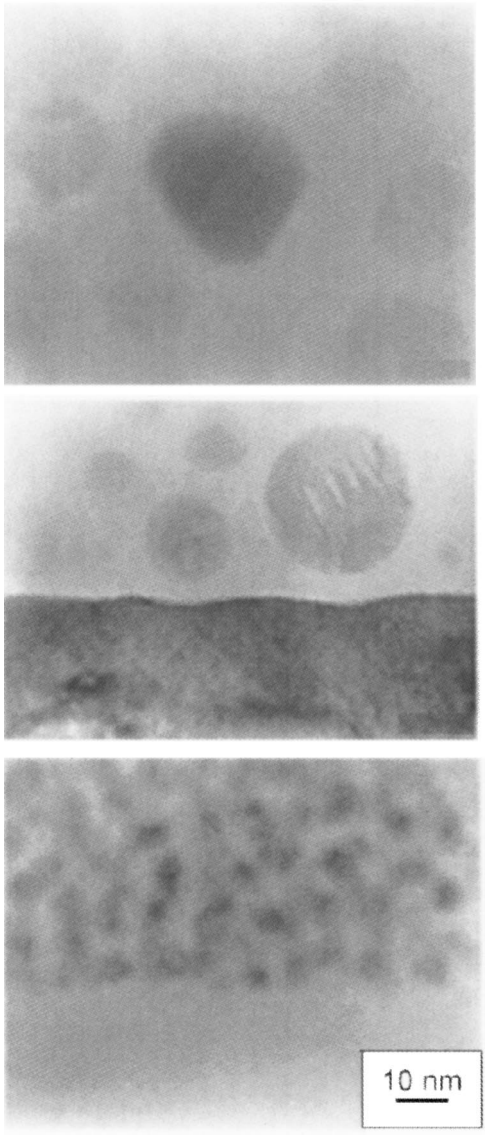

FIG. 2. HR-TEM images of the annealed Ge⟨60⟩/Si(100) sample with Ge nanocrystals formed in the bulk of the sample (top) and in the vicinity of the Si(100) interface (middle), and of the Ge⟨60⟩/quartz sample (bottom).

Interestingly, the size and distribution of the nanocrystals prepared *in a parallel process* grown on quartz glass are quite different from those on Si(100). This is demonstrated in Fig. 2 (bottom). One can clearly see that the size of the nanocrystals in the nc-Ge/quartz sample is considerably smaller and the nanocrystals form a kind of continuous network.

B. X-ray absorption studies

1. Extended x-ray absorption fine structure

Figure 3 summarizes the Ge *K*-edge EXAFS oscillations after subtraction of smooth backgrounds due to the atomic absorption from the fluorescence yield spectra and normalization to the edge jump. The background subtraction has been performed using AUTOBK of the UWXAFS3.0 (Ref. 16)

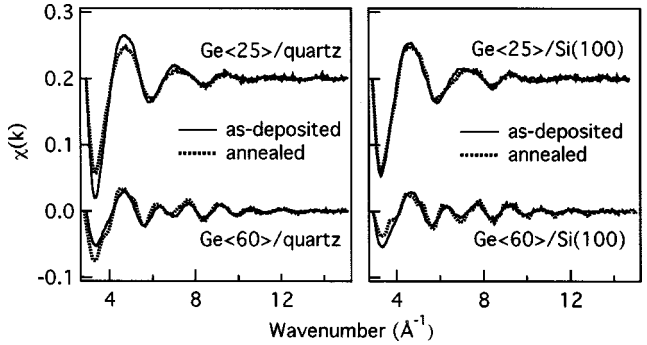

FIG. 3. Raw EXAFS oscillations for as-deposited and annealed samples on quartz substrate (left) and Si(100) (right). The Ge content is shown next to each curve.

and USTCXAFS2.0 (Ref. 17) codes. The figure also shows the modification to EXAFS spectra upon annealing for the nc-Ge/Si(100) (left) and nc-Ge/quartz (right).

One can see that the substrate dependence is not as strong as may be expected judging from the difference observed in the TEM images. Higher amplitude of oscillations at lower wave numbers in samples with low and intermediate Ge concentrations (Fig. 3) indicates that Ge species in those samples are predominantly surrounded by light elements.

The EXAFS oscillations multiplied by k $[k\chi(k)]$ were Fourier-transformed (FT) using the region typically extending from 4 to 16 Å^{-1} and a Hanning window. Figure 4 compares the FT spectra for the as-deposited and annealed samples deposited onto the two substrates. One can see that the spectra consist essentially of two peaks located at 1.7 and 2.4 Å. The peak located at 1.7 Å is due to Ge-O interactions while that at 2.4 Å represents the Ge-Ge interaction. The relative intensity of the Ge-Ge peak increases with an increase in the Ge content. Upon annealing, the intensity of the

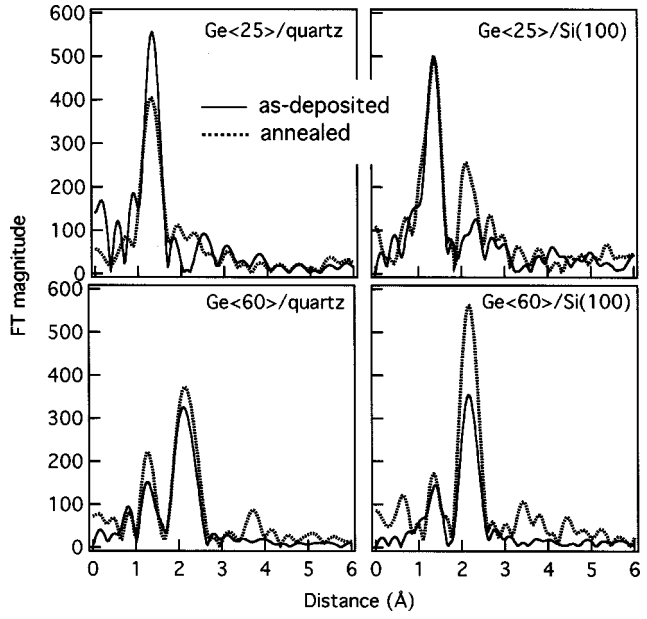

FIG. 4. FT spectra of as-deposited (solid lines) and annealed (dotted lines) samples.

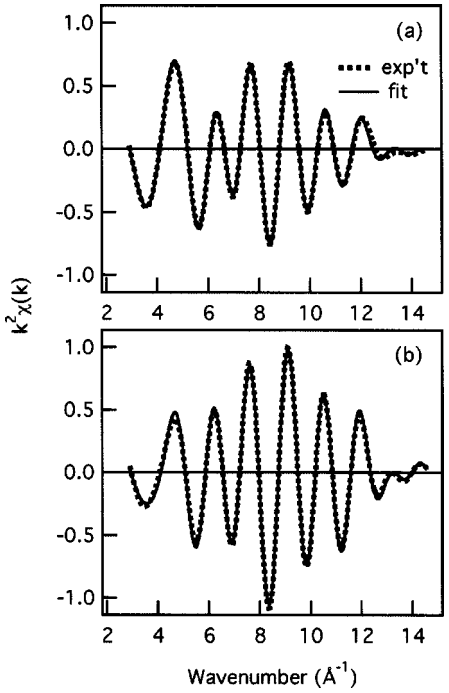

FIG. 5. Fitting examples. Both Ge-O and Ge-Ge shells were used for fitting (R range of 1.0–2.7 Å) the EXAFS spectra of the (a) as-deposited and (b) annealed Ge⟨60⟩/Si(100) samples. Dotted lines, experiment; solid lines, fit.

Ge-Ge peak increases and higher shells appear, which provides evidence of the formation of the crystalline state.

For quantitative analysis, the least-squares curve fit was performed using the USTCXAFS2.0 code,[17] and the theoretical amplitude functions were calculated by FEFF8.[14] The Fourier-transformed data were filtered and back-Fourier-transformed into k space. To achieve better statistics and maximum confidence in the results, the fitting was performed including both Ge-O and Ge-Ge nearest-neighbor correlations in the fit. We did not include Ge-Si correlations in the fit, and the reason for that is discussed in Sec. IV C 1.

The filtered data Ge⟨60⟩/Si(001) samples using the R range including *both* Ge-Ge and Ge-O pairs (1.0–2.7-Å range), together with the result of the least-squares curve fitting based on a single scattering theory, are shown in Fig. 5 to demonstrate the quality of the fit. The obtained good fit quality provides additional evidence that Ge-Si bonds are not present in our samples. Structural parameters obtained for all samples are summarized in Table I.

2. X-ray absorption near-edge structure

Figure 6 (top) shows XANES spectra for as-made samples with different Ge concentration deposited on two different substrates. For comparison, XANES spectra of reference samples, i.e., Ge and GeO_2, are also shown (Fig. 6, bottom). One can see that for the low-Ge-concentration samples there is a substrate dependence, namely, the white line is higher for the case of the Ge⟨25⟩/Si(100) sample. The high-Ge-concentration samples have identical XANES spectra for both substrates.

TABLE I. Summary of the fitting results.

Sample description	Bond type	N	R ($\pm$0.01 Å)	σ ($\pm$0.03 Å^2)
Ge⟨25⟩/Si(100)	Ge–O	4.0±0.3	1.73	0.06
as-deposited	Ge–Ge	<0.2		
Ge⟨40⟩Si(100)	Ge–O	3.1±0.4	1.73	0.07
as-deposited	Ge–Ge	0.7±0.3	2.44	0.07
Ge⟨60⟩/Si(100)	Ge–O	1.5±0.3	1.74	0.06
as-deposited	Ge–Ge	2.5±0.3	2.45	0.07
Ge⟨25⟩/Si(100)	Ge–O	3.6±0.3	1.73	0.05
annealed	Ge–Ge	0.3±0.2		
Ge⟨40⟩/Si(100)	Ge–O	2.9±0.3	1.73	0.06
annealed	Ge–Ge	1.2±0.2	2.45	0.06
Ge⟨60⟩/Si(100)	Ge–O	1.0±0.3	1.73	0.06
annealed	Ge–Ge	3.2±0.3	2.45	0.06
Ge⟨25⟩/quartz	Ge–O	4.2±0.3	1.73	0.05
as-deposited	Ge–Ge	<0.2		
Ge⟨40⟩/quartz	Ge–O	3.9±0.4	1.73	0.05
as-deposited	Ge–Ge	<0.2		
Ge⟨60⟩/quartz	Ge–O	1.3±0.3	1.75	0.06
as-deposited	Ge–Ge	2.4±0.4	2.45	0.07
Ge⟨25⟩/quartz	Ge–O	3.8±0.4	1.73	0.06
annealed	Ge–Ge	<0.2		
Ge⟨40⟩/quartz	Ge–O	4.0±0.4	1.73	0.05
annealed	Ge–Ge	<0.2		
Ge⟨60⟩/quartz	Ge–O	1.4±0.3	1.73	0.05
annealed	Ge–Ge	2.7±0.4	2.45	0.07

Upon annealing, the modification of the XANES spectra strongly depends on the Ge content and the substrate material (Fig. 7). Thus for the Si(100) substrate annealing of the low-Ge-content sample does not lead to any detectable changes. The Ge⟨60⟩/Si(100) sample, on the other hand, exhibit a pronounced change: instead of a broad single-peak white line in the as-deposited sample, two features are clearly observed in the white line of the annealed sample.

In the case of the quartz substrate, annealing of the Ge⟨25⟩ sample results in a significant reduction of the white-line intensity. For the higher Ge concentration, the change is similar to, but not identical to, the Si(100) substrate case. The white line in the annealed sample also exhibits two features, but the intensity of the higher-energy feature is stronger for the quartz-glass substrate than that for the Si(100) substrate. A certain similarity in the spectra for the annealed samples is also observed. The higher-energy feature has the same intensity for the samples with different Ge content, but the spectrum for the high-concentration Ge additionally possesses a shoulder at low energies. Such shoulder is not observed for the low-concentration sample. To summarize, XANES spectra exhibit strong substrate dependence, and their modification upon annealing also strongly depends on the Ge content.

C. Optical studies

1. Raman scattering

For the Ge⟨25⟩ samples, Raman spectroscopy was not able to reveal any Ge-related features. In the samples with the higher Ge content, the formation of Ge nanocrystals upon annealing is also shown by Raman scattering spectroscopy. As an example, we show the spectra for as-made and annealed Ge⟨60⟩ samples on the two different substrates (Fig. 8). A broad feature located around 280 cm^{-1} in the as-made

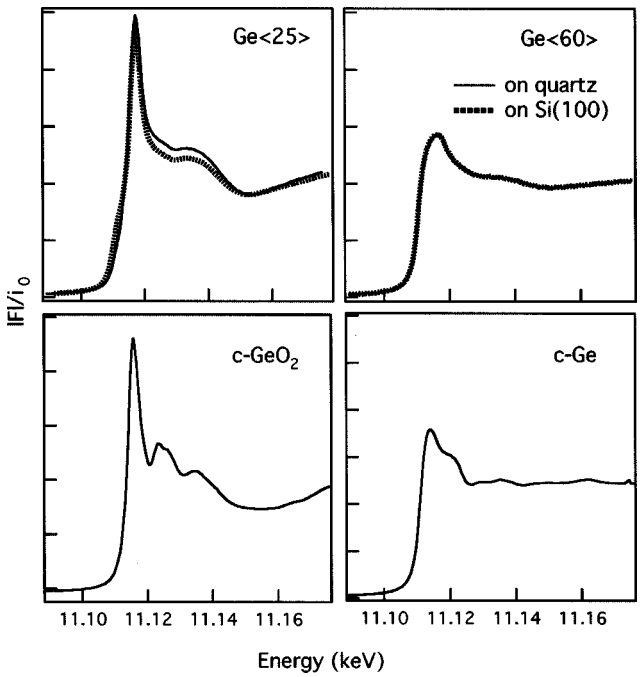

FIG. 6. XANES spectra of as-deposited samples with different low and high Ge content on different substrates (top pair) and XANES of reference samples (bottom pair).

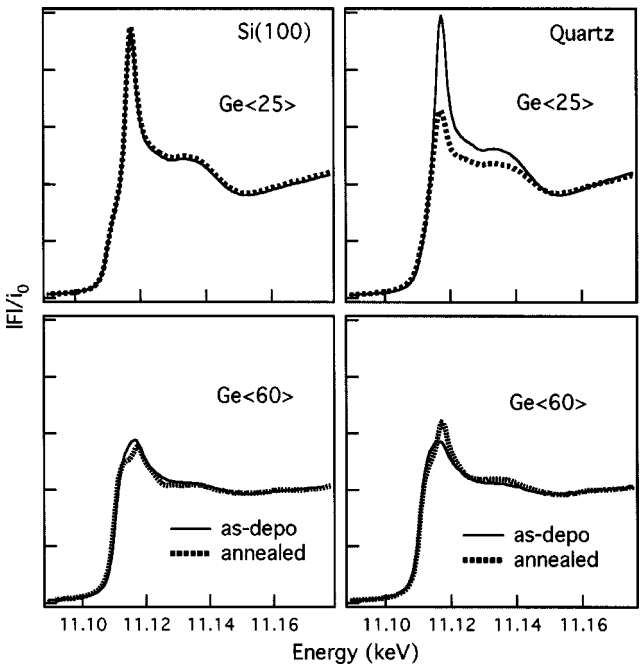

FIG. 7. Modification of XANES spectra for samples with low and high Ge content on different substrates upon annealing. Top pair, Ge⟨25⟩; bottom pair, Ge⟨60⟩; left column, Si(100); right column, quartz substrate.

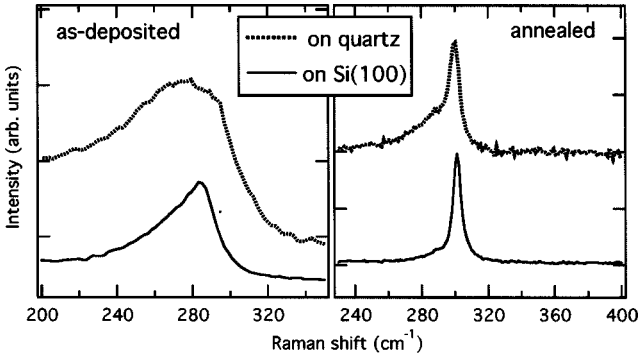

FIG. 8. Raman spectra for as-deposited (left) and annealed (right) Ge⟨60⟩ samples on different substrates (633-nm excitation light). Notice that vertical scales are different for the right-hand side and left-hand side plots.

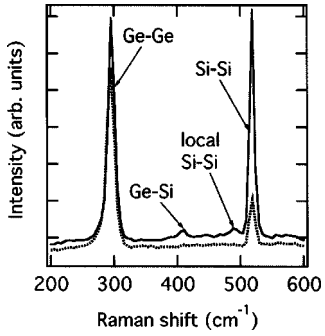

FIG. 9. Polarized Raman spectra for the annealed Ge⟨60⟩/Si(100) sample. Scattering geometries: solid line, $z(xy)z$; dotted line, $z'(x'y')z'$. The unprimed coordinates correspond to usual cube edges; the primed coordinates correspond to a system rotated about [001] axis by 45°.

samples (left) is transformed into a sharp crystalline peak, located at 300 cm^{-1} in the annealed sample (right).

The difference between the samples prepared in a parallel way on two different substrates is clearly seen. Even in as-deposited samples, the peak shape is different. For the Ge⟨60⟩/Si(100) sample the peak has a shape characteristic of the amorphous phase.[7] At the same time the peak for the Ge⟨60⟩/quartz sample is asymmetric and signs of initial crystallization are seen. The difference is also seen in the annealed samples. The nc-Ge peak for the Ge⟨60⟩/Si(100) sample is narrow and almost symmetric. The nc-Ge⟨60⟩/quartz sample, on the other hand, possesses a Raman spectrum characterized by a broader asymmetric peak.

Figure 9 shows the polarized Raman spectra for the nc-Ge⟨60⟩/Si(100). One can see that while the substrate peak is strongly polarized representing the orientational dependence, the Ge-Ge peak intensity does not depend on the scattering geometry. The feature located at 410 cm^{-1}, which is due to Ge-Si vibrations, on the other hand, is polarized in the same way as the Si-Si peak.

2. Optical transmission

Figure 10 compares optical transmission spectra of as-deposited and annealed Ge⟨60⟩/quartz samples. One can see that annealing modifies the transmission spectrum in two ways: the amplitude of interference oscillations increases and the absorption edge becomes less steep.

IV. DISCUSSION

A. Transmission electron microscopy

Evidence of the formation of Ge nanocrystals is directly given by TEM. As mentioned previously, the density of the nanocrystals is the lowest at the surface and there is a denser region in the immediate vicinity of the SiO_2/Si interface (Fig. 1). This is in agreement with some of the previous findings and is explained by diffusion of Ge towards the SiO_2/Si interface.[18,19]

Comparison of the nanocrystal shape in the bulk of the sample and at the interfaces clearly demonstrates the importance of the surrounding. Previously we concluded[20] that the nanocrystals are mainly formed from the preexisting amorphous Ge phase. We believe that this explains the lack of Si alloying. The rather ''soft'' amorphous SiO_2 matrix is a likely reason for the formation of well-faceted nanocrystals.

The Ge atoms located in SiO_2 close to the Si substrate, on the other hand, are under compressive strain. In order to minimize the effect of strain, the nanocrystals tend to minimize the surface energy, the result being a spherical shape with multiple twins. Spherical Ge nanocrystals of similar size and structure have also been reported in Refs. 4 and 21. The nanocrystals located in the vicinity of the substrate have an additional possibility to interact with the substrate. The interface roughness under the nanocrystals suggests Si-Ge intermixing. It is worth mentioning that the above alloying predominantly occurs on the substrate and not in the nanocrystals, as we have found in Raman scattering and as was previously observed by TEM.[21]

The difference in the nanocrystal structure for the different substrate use is further proof of the importance of the interface around the Ge nuclei for nanocrystal formation. At present we do not have an explanation as to why the nanocrystal size and shape differ so much for the Si(100) and quartz-glass substrate.

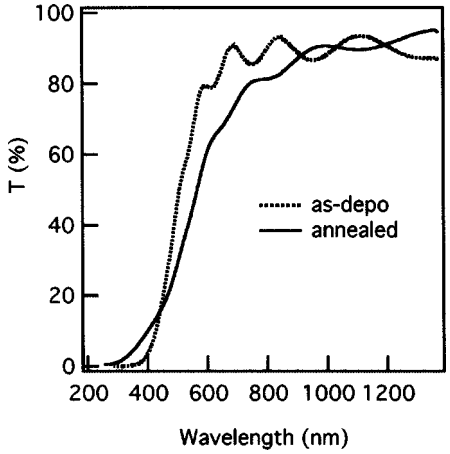

FIG. 10. Optical transmission of as-deposited and annealed Ge⟨60⟩/quartz samples.

B. X-ray absorption study

1. Extended-x-ray absorption fine structure

Raw EXAFS and FT data show that, generally, there are two kinds of correlations, Ge-Ge and Ge-O. In as-made samples with low and intermediate Ge concentrations, Ge-O correlation is dominant. In the high-concentration sample Ge-Ge correlation dominates, but only the signal from the first shell is observed. This result indicates that, although Ge and Si form a continuous solid solution, in the GeO_2-SiO_2 system with Ge concentration exceeding a certain value, phase separation takes place and Ge exists in the amorphous phase (in samples with higher Ge content).

Upon annealing, Ge-O correlations decrease and Ge-Ge correlations increase. In addition, higher shells appear, indicating crystallization of Ge.

The observed bond length in nc-Ge of 2.45 ± 0.01 Å, effectively the same as in bulk Ge, demonstrates that the nanocrystals are relaxed despite a 4% lattice mismatch between Ge and Si. For epitaxial growth, the strain in the bond length was reported to cause Ge–Ge bond compression of 0.03 Å.[22,23] A similar value of Ge–Ge bond compression in epitaxially grown dots were also observed in our previous study.[24] We believe that the difference in the Ge–Ge bond relaxation in epitaxial dots and in embedded nanocrystals is due to the fact that the amorphous SiO_2 matrix is rather ''soft'' and allows for the structural relaxation in the nanocrystals.

Assuming that Ge and Ge-oxide phases are well separated, we can get, based on the fractional coordination numbers, the amount of Ge atoms in the Ge phase to be ~50–60 % in the Ge⟨60⟩ samples. The assumption of the formation of the well-defined Ge phase is based on an observation of Ge features in the Raman spectra. It should be noted, however, that this estimation provides an upper limit value.

The annealing modifies the Ge-O and Ge-Ge peaks differently in different samples (Fig. 4). The curve-fitting results demonstrate that in all samples the partial Ge-Ge coordination number seems to increase very insignificantly (the change being within the error bars); however, we believe that the trend is clear and the observed increase in the Ge-Ge signal for samples on Si(100) upon annealing observed both in Fig. 4 and in the fitting results is real. We do not have any explanation as to why a similar trend is not observed for the quartz substrate. A strong substrate dependence of the nanocrystal formation has been also observed by TEM as described earlier.

2. X-ray absorption near-edge structure

Comparison of the measured XANES spectra with those for reference samples (Fig. 7) demonstrates that generally both oxidized and reduced Ge species are present: the former resulting in the strong white line and the latter producing a shoulder at lower energies. A simple analysis based on deconvolution of the XANES spectra into metallic Ge and GeO_2 spectra allows one to roughly estimate the fraction of Ge atoms in the oxidized state. Precise determination of the fraction of oxidized Ge using XANES is, however, impossible. XANES features are determined by multiple-scattering processes and, provided the size of each phase is comparable to the region in which the multiple scattering takes place, representation of the XANES as a weighted sum of different phase may not be correct.[25]

Several conclusions can, nevertheless, be made. First, the structural modification of the samples strongly depends on the Ge content and the substrate material. For the Si(100) case, annealing does not seem to produce any significant changes for the low-Ge-content sample. For the high-Ge-content sample, the two features are resolved in the white line. This change may represent the formation of better phase separation as a result of annealing. Indeed, for the strongly intermixed Ge-O and Ge-Ge phases one should expect a broad featureless white line. In the sample with well-defined phases, the characteristic size of each being larger than the characteristic size of the multiple-scattering region, the XANES can be presented as a weighted sum of the constituent phases. Assuming the latter (and knowing from TEM that the nanocrystal size is ~20 nm), we can estimate the fraction of the Ge phase to be ~60%, which agrees with the results of EXAFS data analysis.

For the quartz-glass substrate, the situation is quite different. The white line in the low-Ge-content sample is greatly decreased after annealing, clearly demonstrating the reduction of Ge oxide. This result is in good agreement with previous conclusions.[6] For the high-Ge-content sample, the white line *increases* after annealing. This result may be indicative of the formation of the oxide but also of the spatial redistribution of Ge species. Assuming that rather large amorphous Ge regions form small-size nanocrystals, one can expect an increase in the fraction of the surface atoms. Since the surface atoms are coordinated by oxygen atoms, such structural modification should result in an increase of the oxide white-line intensity. We believe that this is the reason for the increase of the white line in our case. The small size of the nanocrystals detected by TEM confirms this conclusion.

The observed differences suggest somewhat different mechanisms of the nanocrystal formation in samples with low and high Ge content. While the nanocrystals in the lower-concentration samples may be formed primarily through reduction of Ge oxide and rearrangement of the whole matrix, in high-concentration samples the process may predominantly consist in crystallization of preexisting amorphous Ge.

C. Optical studies

1. Raman scattering

In samples with low Ge content the Ge-Ge peak is absent in both As-deposited and annealed samples. Most likely, this is due to the fact that the concentration of Ge–Ge bonds is low, other neighbors of Ge atoms involved in Ge–Ge bonding being oxygens. In samples with a high Ge content, a broad feature observed in as-made samples is due to amorphous Ge. It should be stressed, however, that the Ge⟨60⟩/quartz sample, in addition to the broad amorphous feature, possesses another feature that is most likely due to very

small nanocrystals. Following Ref. 26 we can roughly estimate the size of these nanocrystals to be around 2–3 nm.

The appearance of strong and sharp peaks upon annealing represents the formation of the crystalline phase. The peak position (299 cm^{-1}), somewhat lower than that in bulk Ge, suggests confinement of phonons in nanocrystals. Since the stress in nc-Ge is negligible (the observed Ge–Ge bond length is the same as that in bulk Ge), the small difference in the peak positions for nc-Ge and bulk *c*-Ge allows us to conclude that the confinement is quite weak, which is reasonable for the 20-nm nanocrystals.

The symmetric line shape for the nc-Ge⟨60⟩/Si(100) sample shows a rather large size of the Ge nanocrystals. The asymmetric shape of the peak obtained for the nc-Ge⟨60⟩/quartz sample is characteristic of the small crystals. The crystal size estimated from the peak full width at half-maximum (FWHM) using the calibration curves from Ref. 27 yields the crystal size of 3–7 nm, which agrees well with the results of TEM imaging.

The absence of the polarization dependence of the Ge-Ge peak suggests that the nanocrystals are randomly oriented. The fact that the Ge-Si feature exhibits a strong polarization dependence, similar to that of the substrate peak suggests that Ge-Si alloying only takes place at the interface with the Si(100) substrate. Since the nanocrystals located at the Si(100) interface are clearly separated from the substrate (Fig. 2, middle image) and are not epitaxial with respect to it, we conclude that the Ge-Si signal is coming from the very surface of the substrate that becomes alloyed with Ge as a result of annealing. Based on the above arguments, we believe that the formed nanocrystals *per se*, both those in the bulk of the SiO_2 layer and at the Si(100) interface, consist of pure Ge without any Ge-Si alloying. It is this result that allowed us to neglect the Ge–Si bonds in the EXAFS fitting.

2. Optical transmission

The observed changes in the amplitude of oscillations in the optical transmission spectra indicate a decrease in the *nd* (*n* is the refraction index and *d* the thickness) of the annealed film. Direct measurements of the film thickness have shown that the thickness decreased by about ~15% after annealing, i.e., the density of the film increased.

More important is the observed change of the slope of the absorption edge. Since the SiO_2 matrix is completely transparent in this spectral region, the observed change is entirely due to the changes in the electronic structure of Ge. It has been argued that small Ge nanocrystals should possess a direct optical gap[6] and thus a steeper absorption edge. Our experiment shows that upon the formation of the nanocrystals the change is the opposite. We believe that the observed change indicates that the nanocrystal size in our sample (5 nm) is too large for the modification of the band structure. The as-deposited sample, on the other hand, may possess much smaller nanocrystals that could not be detected by EXAFS (because the majority of Ge atoms form the amorphous phase) but were detected by Raman scattering. These nanocrystals may account for the steeper absorption edge. This result also agrees with the conclusion that for the direct optical band to be formed the size of the nanocrystals has to be less than 4 nm,[28] and in addition it was suggested[28,29] that such small nanocrystals should have ST-12 rather than the diamond structure in order to produce efficient PL.

This explanation agrees with the recent PL studies on the same set of samples.[30] The PL intensity was the strongest in as-deposited samples and much weaker in the annealed samples. Assuming that efficient PL is due to quantum confinement,[6] one would expect stronger PL in smaller nanocrystals that are likely to exist in the as-deposited Ge⟨60⟩/quartz sample. We would like to stress here that the origin of strong PL in Ge nanocrystals embedded in SiO_2 remains a matter of controversy and further experiments are needed to draw the final conclusions.

V. CONCLUSIONS

We have performed comparative TEM, x-ray absorption, and Raman scattering studies on as-deposited and annealed Ge/SiO_2 samples prepared in a parallel way on quartz-glass and Si(100) substrates. We found that annealing results in the formation of Ge nanocrystals, their size and configuration strongly depending on Ge content and the substrate material. In the particular case of Ge⟨60⟩/Si(100) samples, the formed nanocrystals are ~20 nm in size and can be either faceted or spherical, depending on their location in the matrix. The Ge–Ge bond length in the nanocrystals (2.45 Å) is the same as that in bulk *c*-Ge, i.e., the nanocrystals are relaxed. The formation of the nanocrystalline phase has been also detected by Raman scattering. A small shift in the Ge-Ge peak position is attributed to weak phonon confinement in the nanocrystals.

ACKNOWLEDGMENTS

This work, partly supported by NEDO, was carried out at Joint Research Center for Atom Technology (JRCAT) under a research agreement between AIST and Angstrom Technology Partnership (ATP).

*On leave from A.F. Ioffe Physico-Technical Institute, St. Petersburg, Russia. Electronic address: a.kolobov@aist.go.jp

[1] L. Pavesi, Nature (London) **408**, 440 (2000).
[2] H. Rinnert, M. Vergnat, and A. Burneau, J. Appl. Phys. **89**, 237 (2001).
[3] S. Banerjee, S. Nozaki, and H. Morisaki, Appl. Phys. Lett. **76**, 445 (2000).
[4] W. K. Choi, W. K. Chim, C. L. Heng, L. W. Teo, V. Ho, V. Ng, D. A. Antoniadis, and E. A. Fitzgerald, Appl. Phys. Lett. **80**, 2014 (2002).
[5] T. Takagahara and K. Takeda, Phys. Rev. B **46**, 15 578 (1992).
[6] Y. Maeda, Phys. Rev. B **51**, 1658 (1995).
[7] M. Zacharias, J. Blasing, J. Christen, P. Veit, B. Dietrich, and D. Bimberg, Superlattices Microstruct. **18**, 139 (1995).
[8] V. Craciun, I. W. Boyd, A. H. Reader, and E. W. Vandenhoudt, Appl. Phys. Lett. **65**, 3233 (1994).

[9] K. L. Teo, S. H. Kwok, P. Y. Yu, and S. Guha, Phys. Rev. B **62**, 1584 (2000).
[10] A. Saito and T. Suemoto, Phys. Rev. B **56**, R1688 (1997).
[11] D. Dimova-Malinovska, N. Tzenov, and M. Tzolov, Bulg. J. Phys. **21**, 80 (1994).
[12] A. V. Kolobov, J. Appl. Phys. **87**, 2926 (2000).
[13] A. V. Kolobov, J. Vac. Sci. Technol. A **20**, 1116 (2002).
[14] A. Ankudinov, B. Ravel, J. J. Rehr, and S. D. Conradson, Phys. Rev. B **58**, 7565 (1998).
[15] A. V. Kolobov, H. Oyanagi, K. Tanaka, and K. Tanaka, Phys. Rev. B **55**, 726 (1997).
[16] M. Newville, P. Livins, Y. Yakoby, J. J. Rehr, and E. A. Stern, Phys. Rev. B **47**, 14 126 (1993).
[17] W. Zhong and S. Wei, J. Chin. Univ. Sci. Technol. **31**, 228 (2001).
[18] H. Fukuda, T. Kobayashi, T. Ehndoh, and Y. Ueda, Appl. Surf. Sci. **130-132**, 776 (1998).
[19] K. H. Heining, B. Schmidt, A. Markwitz, R. Grotzschel, M. Strobel, and S. Oswald, Nucl. Instrum. Methods Phys. Res. B **148**, 969 (1999).
[20] A. V. Kolobov, H. Oyanagi, Y. Maeda, and K. Tanaka, J. Synchrotron Radiat. **8**, 511 (2001).
[21] W. K. Choi, Y. W. Ho, S. P. Ng, and V. Ng, J. Appl. Phys. **89**, 2168 (2001).
[22] J. C. Aubry, T. Tyliszczak, A. P. Hitchcock, J.-M. Maribeau, and T. E. Jackman, Phys. Rev. B **59**, 12 872 (1999).
[23] J. C. Woicik, J. G. Pellegrino, B. Steiner, K. E. Miyano, S. G. Bompadre, L. B. Sorensen, T. L. Lee, and S. Khalid, Phys. Rev. Lett. **79**, 5026 (1997).
[24] A. V. Kolobov, H. Oyanagi, S. Wei, K. Brunner, G. Abstreiter, and K. Tanaka, Phys. Rev. B **66**, 075319 (2002).
[25] A. Kolobov, H. Oyanagi, N. Usami, S. Tokumitsu, T. Hattori, S. Yamasaki, K. Tanaka, S. Ohtake, and Y. Shiraki, Appl. Phys. Lett. **80**, 488 (2002).
[26] M. Zacharias, R. Weigand, B. Dietrich, F. Stoltze, J. Blasing, P. Veit, T. Drusedau, and J. Christen, J. Appl. Phys. **81**, 2384 (1997).
[27] W. K. Choi, V. Ng, S. P. Ng, H. H. Thio, Z. X. Shen, and W. S. Li, J. Appl. Phys. **86**, 1398 (1999).
[28] Y. Kanemitsu, H. Uto, Y. Matsumoto, and Y. Maeda, Appl. Phys. Lett. **61**, 2187 (1992).
[29] S. Saito, S. Nozaki, and H. Morisaki, Appl. Phys. Lett. **72**, 2460 (1998).
[30] T. V. Torchynska, J. Aguilar-Hernandez, L. Schacht-Hernandez, G. Populan, Y. Goldstein, A. Many, J. Jedrzejewski, and A. V. Kolobov, Microelectron. Eng. (to be published).